2024 IEEE International Conference on Robotics and Automation (ICRA 2024)
May 13-17, 2024. Yokohama, Japan

Robotic capillary insertion to the Xenopus oocyte using microscopic image analysis and QCR force sensor

Kazusa Otani, Hirotaka Sugiura, Shiro Watanabe, Turan Bilal,
Satoshi Amaya, Fumihito Arai, *Member IEEE*

Abstract— **This paper presented the three-dimensional oocyte manipulation system for the two-electrode voltage clamp (TEVC) experiment under stereomicroscopy. We firstly developed a sequential calibration method to correlate the workspace of the stereomicroscopy with the image and the micromanipulator. Even though the focal depth of the microscopy was limited, the proposed method functioned the three-dimensional position detection and calculated the homogeneous transformation matrix. We secondly employed hybrid use of the image-based manipulation and the quartz crystal resonator (QCR) force sensor. The imaging technique was used to detect the tip of the glass capillary and the contact to the cell membrane, whereas the QCR force sensor was incorporated to detect the force interaction between the sample and the glass capillary. Using the system and proposed technique, we demonstrated the automatic capillary insertion for TEVC experiment, at which the low insertion depth was preferable. The results indicated that the coordination calibration technique provided the positioning accuracy of the capillary tip on the order of 10 μm. The imaging technique could detect the contact to the elastic objects and cell membrane. QCR force sensor achieved quite small force measurement and feedback control at the control frequency of 100 Hz without latency.**

I. INTRODUCTION

With the recent development of robot micromanipulation technology, automation of experimental tasks using robot systems has attracted attention in biological experiments concerning cells and tissues to improve the experimental reproducibility and the throughput of the screening experiment [1-2]. A representative experiment that requires robot automation is the electrophysiological analysis which elucidates the kinetics of the ion channels using a two-electrode voltage clamp (TEVC) [3]. Using TEVC, scientists elucidate the medicinal and toxic effect of the organic compounds, or even explore a new compound [4-5]. In the TEVC experiment, a couple of fine glass capillary electrodes are inserted into the Xenopus oocyte on which the target channel is expressed, and the electrical response such as the membrane potential or the ionic current are measured [6]. TEVC visualize the gating performance of the ion channels modulated by the compounds acting on their binding sites. In contrast, the insertion task of the glass capillary probes is so difficult that human operators generate the large experimental errors unless they are well trained and concentrated. The glass capillary must be inserted into the soft oocyte membrane uniformly and with the shallow penetration depth to prevent the large current leakage [7]. In addition, since there are large individual differences in cell conditions, such as the size and membrane stiffness, making it difficult to realize the reproducible manipulation.

In order to automatically perform the TEVC experiment, some groups invented an integrated system for the capillary insertion [8]. Using the high precision of the robot stages, and microfluidic control of the cells, highly accurate and high throughput capillary insertion to the oocyte was achieved. However, the system does not have the redundancy of the experimental tasks. TEVC experiment requires numerous tasks such as the gene primer injection for the channel expression, cell loading depending on the cell quality, and applying the compounds for each logarithmic concentration with numerous conditions [7]. For the truly automatic or even autonomous operation of TEVC with high precision, these complex tasks should be performed in a single platform

Therefore, we designed an automated platform that integrated a dual-hand 3-D translational robot manipulator, force sensor unit on the fluidic environment under stereomicroscopy. The system concept is the non-specific manipulation platform to perform the versatile task all by itself. On the other hand, the controllability of the stages, actuators and the sensors have the state-of-art performance to perform the versatile micromanipulations including the TEVC experiment. To realize this concept, there are two major points. The first point is the 3D calibration of coordination in the limited focal depth of the stereomicroscopy. In the TEVC experiment, the two glass capillaries should be inserted from the ex-planar direction, which caused large positioning error unless the workspace was not calibrated. Therefore, we developed the 3D position detection method based on the capillary contact to the soft pillar. The second is the accurate control of the interactions between the glass capillary and oocyte samples so that the penetration depth is as small as possible [7]. This requires accurate detection of membrane deformation based on microscopic image analyses, and quite small force sensing on the order of several μN, keeping structural rigidity high to endure the fluidic disturbance. We therefore developed a QCR cantilever force sensor that exhibited high sensitivity and rigidity simultaneously [9]. For the feed-back control of the small force without any latency, we configured the real-time signal detection technique of the QCR. Finally, by integrating these techniques into the system, we achieved the insertion task of the capillary penetration.

K. Otani, H. Sugiura, S. Watanabe, S. Amaya, and F. Arai are with the Department of Mechanical Engineering, Graduate School of Engineering, The University of Tokyo, Japan. (corresponding author e-mail: hsugiura965@g.ecc.u-tokyo.ac.jp, and the principal investigate email : arai-fumihito@g.ecc.u-tokyo.ac.jp).

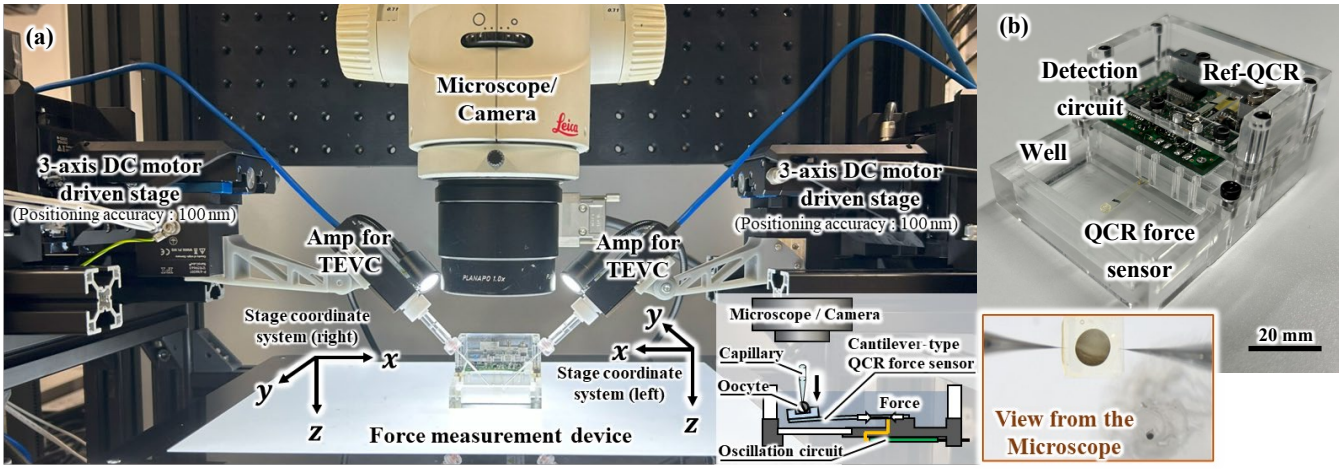

Fig. 1 (a)The system overview for the micromanipulation system of TEVC experiment under the stereomicroscopy; All of the system components were fastened by the aluminum frame on the stainless base. The stage coordination was expressed in the diagram. The arm structures were configured by the 3D-printed material so that the complex truss structures could be easily fabricated. For the TEVC experiment, the electrophysiological amplifier (AXOCLAMP-900/MolecularDevices. Inc) was clamped. (b) The focus image of the microfluidic well device; The QCR force sensor was embedded, and liquid exchange was available for the screening experiment by using the manual pump.

II. System Overview and Methodologies

A. Total System Design

Figure 1(a) shows an overview of the system. The system was configured by the dual 3-D positioning stage (F-712.MA2 /physikinstrumente (PI), Inc.), stereomicroscopy (M-105/ Leica, Inc.) microfluidic well and the QCR force sensor. Both the transparent and epi-illumination are placed to provide good contrast of the images. The CMOS image sensor was 8-bit monochrome with an area of 1024x768, purchased from Basler Inc. Image distortion and magnification were compensated by the microscope for the movement of the Z-focus. The DC motors of the translation stages moved 25 mm with a resolution of 0.1 μm for each of the axes. At the tip of the motor stage, the 3D-printed arm structures held the TEVC amplifier with sufficient stiffness. The microfluidic well was placed on the workspace to load and the microarm structure measured the characteristics of the oocyte. At the bottom of the oocyte, the QCR cantilever force sensor with the waterproof coating was placed. At the tip of the cantilever, the glass block with the 2 mm dimple was glued to accommodate the oocyte. The QCR force sensor exported the frequency output whose carrier frequency was 38 MHz. When the force was applied to the oscillator, the oscillation frequency was modulated and detected by the real-time signal detection board. The environment of the oocyte measurement was shown in Figure 1(b). The oocytes were placed one by one on the measuring point by the external pipette [10], and the glass capillary was inserted at an angle of 45 degrees from the working plane.

B. The coordination calibration technique

In order to handle the samples and insert the glass capillary in three dimensions with high precision, it is necessary to map the spatial coordination system of the microscope, the working plane and the manipulator as a homogeneous transformation matrix. In general, 3D calibration has been performed by using stereovision, Time-of-flight (ToF) image sensors, or some 3D measurement architecture such as interferometry. In contrast, in the microscopic field, the working space is limited and the focal depth is shallow. Therefore, it is difficult to obtain the 3D position accurately on the order of several micrometers at a time. In addition, in the workspace for manipulating the biological sample, the liquid-air interface would cause unexpected reflection, which made it difficult to implement the sophisticated optical system. Therefore, we separated the calibration process for the XY image plane versus manipulator, and the Z-axis base-level detection and 3D workspace versus manipulator, respectively, as shown in Figure 2. First, the position of the XY image plane was detected by the corner detection algorithm developed by Shi-Tomasi [11]. By applying the correct displacement to the XY stage and obtaining the encoder values, we correlated as a 2-D homogeneous transformation matrix, $\widehat{\boldsymbol{H}}_{pq}$, expressed as the following equation.

$$\widehat{\boldsymbol{H}}_{pq} = \left(\widehat{\boldsymbol{P}}^T\widehat{\boldsymbol{P}}\right)^{-1}\widehat{\boldsymbol{P}}^T\widehat{\boldsymbol{Q}}, \tag{1}$$

where the $\widehat{\boldsymbol{P}} = \left[\boldsymbol{x}_p, \boldsymbol{y}_p, 1\right]^T$ and $\widehat{\boldsymbol{Q}} = \left[\boldsymbol{x}_q, \boldsymbol{y}_q, 1\right]^T$ were the frame of the glass capillary and the image, respectively.

The position along the Z direction was subsequently detected by the contact of the glass capillary against a soft pillar made of polydimethylsiloxane (PDMS). The pillars were installed in the experimental environment by the bonding adhesive. Now that $\widehat{\boldsymbol{H}}_{pq}$ was available, the capillary tip accurately approached exactly over the pillar. As the glass pipette approached downward and made contact with the pillars, the pillar caused the buckling deflection, resulting in the change of the top area of the pillar. Figure 3(a) shows a representative image to detect the contact of the pillars. The contact state was measured by the backward difference of the images, I_{D_i}, expressed as follows.

$$I_{D_i} = \sum_S |I_i(x,y) - I_{i-1}(x,y)|, \tag{2}$$

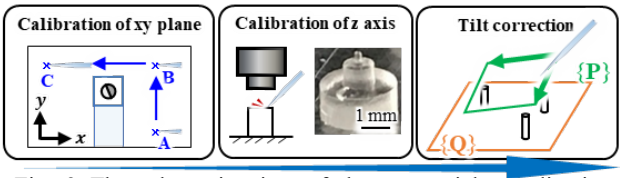

Fig. 2 The schematic view of the sequential coordination calibration; The image frame and the workspace were first correlated, and the Z position and tilt were measured by the contact to PDMS pillars. The XY-planar position and angle are calibrated for each of the insertion process

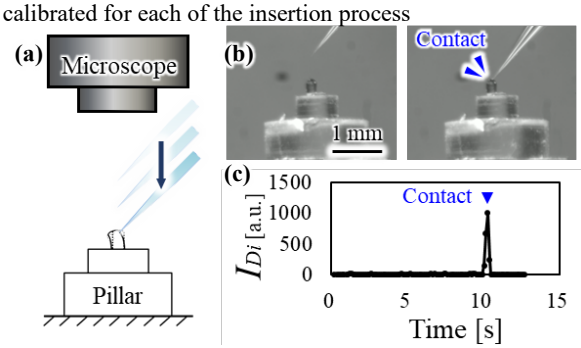

Fig. 3 The contact detection using the PDMS pillar and imaging; (a) the overview ;(b) The front view during the capillary approach; (c) The result of the intensity change; The intensity is corresponding to the buckling of the pillar.

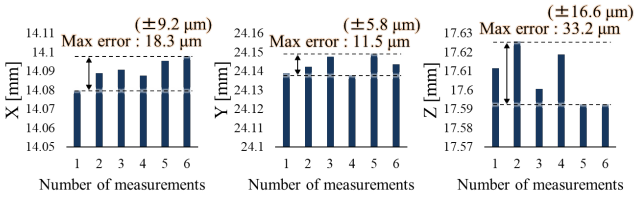

Fig. 4 The repeatability results of the capillary tips for each of the stage axes.

where the $I_i(x, y)$ is the intensity of the image at (x, y) at the timestep of i. Herein, the region of interest (ROI) was determined by the initial pillar surface. To confirm the contact, we placed the macroscope in front of the workspace. The result clearly illustrated that the I_{D_i} was in consistent with the contact state, at shown in Figure 3(b-c). By applying this sequence to the three pillars, we obtained the actual position of pillar top as $\boldsymbol{P} = [\boldsymbol{x_p},\ \boldsymbol{y_p},\ \boldsymbol{z_p}, 1]^T$. Since the pillar position was measured by the laser microscopy (Olympus Co., Ltd.) as $\boldsymbol{M} = [\boldsymbol{x_M},\ \boldsymbol{y_M},\ \boldsymbol{z_M}, 1]^T$, the 3D homogeneous transformation matrix for capillary frame and the workspace $\boldsymbol{H}_{PM}$ was expressed as

$$\boldsymbol{H}_{PM} = (\boldsymbol{P}^T\boldsymbol{P})^{-1}\boldsymbol{P}^T\boldsymbol{M}. \tag{3}$$

Note that the microfluidic device was the removable module for the cleaning. We therefore calculated $\widehat{\boldsymbol{H}}_{pq}$ every time we started with the experiment, and updated the 2D offset and rotational elements of $\boldsymbol{H}_{PM}$ with those of $\widehat{\boldsymbol{H}}_{pq}$.

The performance of the positioning accuracy subjected by the result of the calibration was evaluated as shown in Figure 4. The error was calculated from the absolute value of the encoder. From the results, the XY positioning errors were on the order of 10 μm, and the Z positioning error was slightly large but comparable to the XY positioning error. Given that

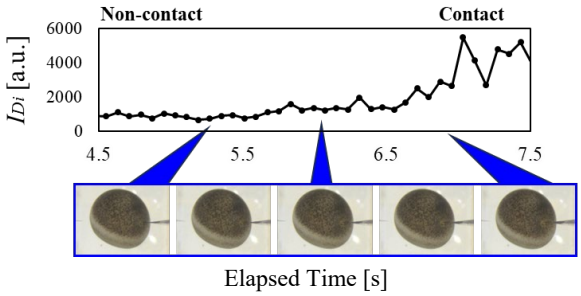

Fig. 5 The image at the neighbor of the exact contact time; When the glass capillary and the oocyte made contact, the image intensity is dramatically changed.

the size of the oocyte was approximately 1 mm, the error was approximately a few percent, mentioning that sufficiently precise positioning of the glass capillary was achieved.

C. The contact and penetration detection

The contact and the penetration of the glass capillary toward the oocytes were detected by using the image analysis and the QCR force sensor. At the beginning of the contact between the glass capillary and the oocyte, the position of the oocyte was slightly moved inside the hole, and the membrane deformation was exerted until the penetration occurred. This change could also be extracted as the intensity change of the ROI of the oocyte, which was calculated by the Hough transformation [12]. Herein, in order to eliminate the effect of the capillary approach from the ROI, a pair of the half elliptic ROI was utilized in this experiment. Figure 5 shows how the ROI was set and the difference from the circular ROI. The result suggested that the effect of the capillary approach was not included in the result, mentioning that the exact time of the contact between the glass capillary and the oocyte was detected.

Although the image processing detected the contact of the glass capillary and the oocyte, the signal was not a quantitative value because the size and membrane elasticity varied depending on the oocyte condition. For the reproducible operation of the capillary insertion into the oocyte, we used the force signal from the QCR force sensor. The QCR force sensor was composed of the thin quartz oscillator with the thickness of 41.7 μm packaged with the 20 μm and 100 μm quartz crystal and photopatternable polyimide adhesive. Figure 6(a) shows the structure of the QCR force sensor. In the oscillation region the circular electrode was deposited on both sides of the oscillator, and the oscillation of thickness-shear mode was generated by connecting the inverter circuit. The feedthrough of the electrode was placed at the edge of the cantilever structure, and the terminals are connected by the silver conductive composite with the epoxy sealing material. The QCR force sensor detected the vertical force using the stress concentration at the root of the cantilever, the oscillation region. Since the oscillator region was out of the neutral plane, the tensile or compressive force was acted on the oscillator. The fabrication process of the oscillator was in similar to that reported before [9]. We therefore briefly explain the process. The overview of the fabrication process was depicted in Figure 6(b). First, the blank of the AT-cut quartz crystal wafer was cleaned by using the organic solvent and sulfuric acid-hydrogen peroxide mixture. The oscillator electrodes were deposited by the sputtering deposition with the stencil mask

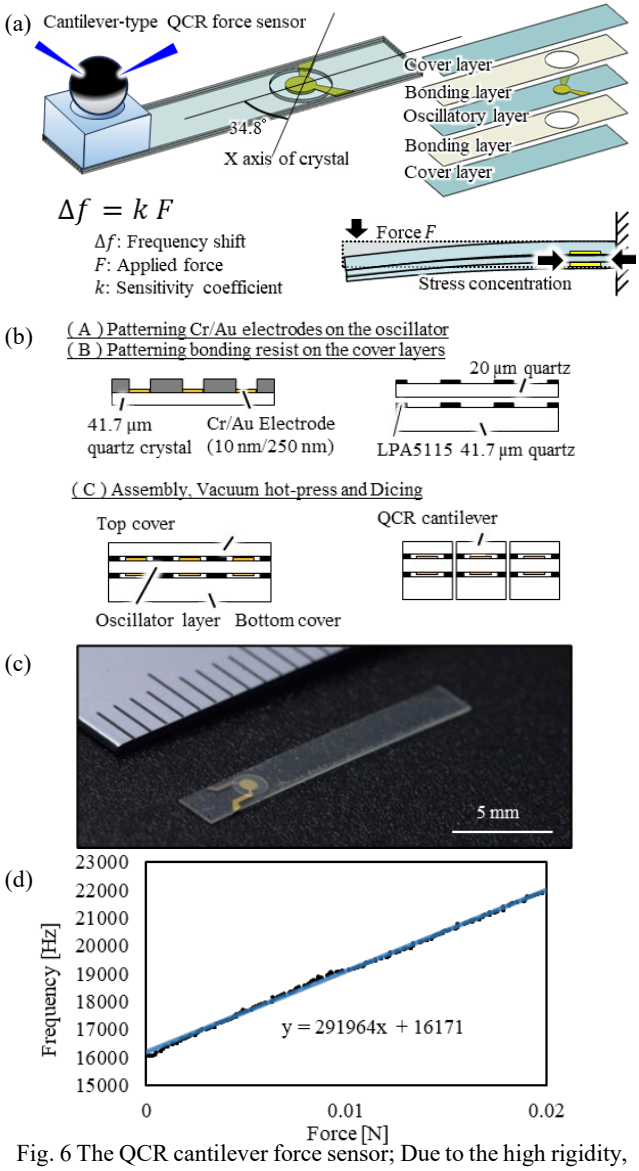

Fig. 6 The QCR cantilever force sensor; Due to the high rigidity, the flapping displacement of the QCR cantilever is several micrometer even if we load the force of several mN; (a) The overview of the sensor structure and the principle to detect the force; (b) The process flow of the QCR force sensor; (c) The fabricated QCR cantilever; (d) The result of the force versus frequency calibration. The result was in proportional to the applied load.

made of silicon. The bonding adhesive (LPA-5115/ Toray) was patterned on the cover layer. These layers are immediately piled up and bonded under the vacuumed and heated environment. Finally, by forming the rectangular shape using the blade dicer, we obtain the QCR cantilever force sensor, as illustrated in Figure 6(c). The calibration result of the frequency shift versus the applied force was illustrated in Figure 6(d). The force reference was a load cell (LTS-50/Kyowa Co., Ltd.) and the frequency shift was measured by the specified detection board. The result exhibited that the frequency shift was linearly proportional to the applied load, and the sensitivity coefficient was 2.92×10^6 Hz/N. Since the frequency noise level of the QCR was less than 1 Hz, the force resolution reached 0.34 μN. Notice that the detected frequency was downclocked to the difference from the

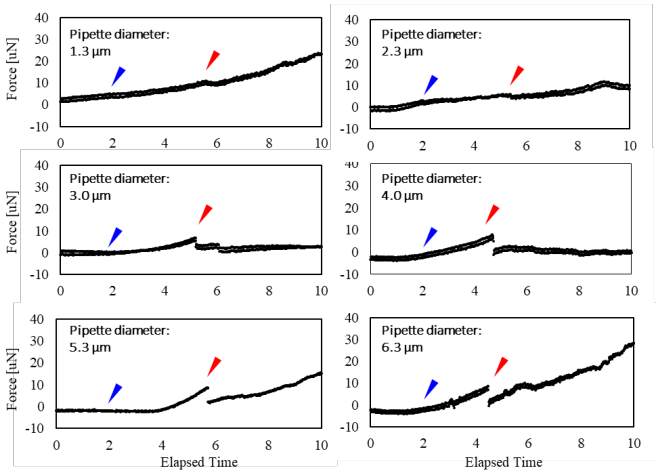

Fig. 7 The results of the force measurement using QCR force sensor; The force dropdown was clearly distinguished when the capillary over 3 μm in diameter penetrated the oocyte membrane.

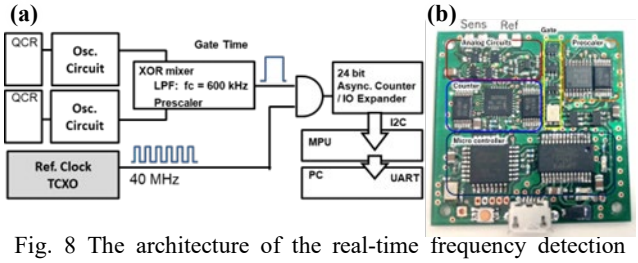

Fig. 8 The architecture of the real-time frequency detection board; The board was specified for the frequency detection without latency, less than 10 ms.

reference QCR with no load. The carrier frequency was therefore trimmed from the resultant frequency, as explained later.

Using the QCR force sensor, we investigated the contact and the penetration force. Since the force is strongly dependent on the tip diameter of the capillary tube, we investigated in some representative cases. Figure 7 shows the contacts and penetration forces measured by the QCR force sensor. In this experiment, the capillary was kept moving to the penetration direction into oocyte for 100 μm/s. The result illustrated that the repulsive force was on the order of several μN, and the capillary over 3 μm in diameter generated the ramp up of the contact signal and sudden drop down of the penetration signal. The slope of the ramp up seemed to be difficult to distinguish from the drift of the QCR sensor. In addition, the contact point did not have the reproducibility due to the translation or rotation of the oocyte. In contrast, the drop-down signal at the membrane penetration quantitatively expressed the force of the puncture. Therefore, we used the QCR force sensor for the quantitative penetration detection of the oocyte membrane. Since the glass capillary tube with a tip diameter of approximately 3 μm is compatible with the TEVC experiment from the viewpoint of the buffer leakage inside the capillary, the proposed method was compatible method to the TEVC experiment. On the other hand, the repulsive force was growing up after penetration. This result suggested the oocyte would be damaged unless the indentation was stopped by the real-time force feedback.

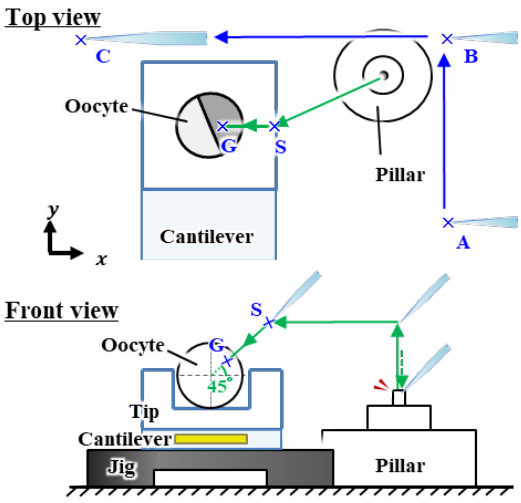

Fig. 9 The trajectory of the capillary tip for the capillary insertion; For the simplicity, we describe only one manipulator in this diagram. Notice that the front view could not be obtained in actual platform since the oocyte sample was soaked into the buffer medium.

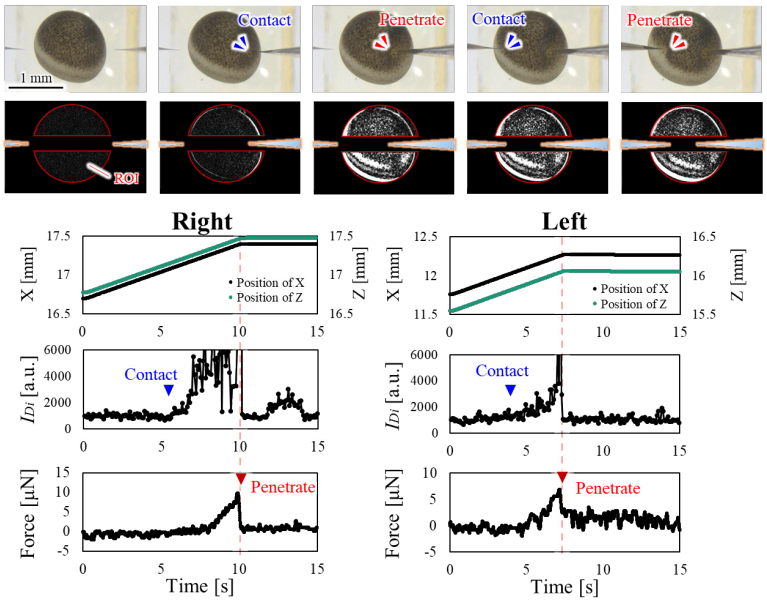

Fig. 10 The experimental demonstration of the capillary insertion; The top images are the bright field images, and the backward differences were depicted below. The encoder values, the Image intensity, and the force signal was plotted. By measuring the force drop down and stop the stages, we succeeded in penetrating the oocyte membrane with the shallow indentation depth.

For the feedback control of the force signal measured by the QCR force sensor, one critical issue was the latency of the universal frequency counter, which would delay approximately 1 s after the frequency detection. For the real-time detection without latency, we developed a detection circuit that employed the reciprocal frequency counter technique [13] having the asynchronously triggered discrete counter. Figure 8(a) illustrated the architecture of the frequency detection circuit. First, the QCR force sensor and the same QCR reference sensor was driven by the CMOS inverter (NJU6385/ Nissinbo Co., Ltd.) and mixed by the exclusive-OR logic (SN74LVC1G86/ Texas Instruments. Inc). By applying the low-pass filter with Butterworth characteristics and 600 kHz cur-off, the frequency difference was obtained. The previous attempt directly read the signal using the counter register of the microprocessor unit. However, the architecture could not realize the uniform sampling rate. The signal was therefore interpolated afterward and low-pass filter should be incorporated. In this study, we generated the gate time using the mixed signal and pre-scaler, keeping the gate time close to the sampling rate. In addition, by using the external temperature-compensated crystal oscillator as the reference clock at 40 MHz, we realized the reciprocal counting system. To latch the counted signal for each sampling period of 10 s, we also utilized the asynchronous counter (SN74LV4040A Texas Instruments. Inc) and the I/O expander (PCAL6524, NXP Inc.). The digitized signal was immediately transported to the control PC, and we succeeded in measuring the frequency shift with little latency, less than the sampling frequency of 10 ms. The fabricated circuit board is shown in Figure 8(b).

III. Experiment of the Capillary Insertion

Using the coordination calibration technique at the workspace of the stereomicroscopy and the contact/penetration detection by using the image analysis and the QCR force sensor, we demonstrated the capillary insertion into the oocyte. First, we designed the trajectory of the capillary as illustrated in Figure 9. The designed trajectory and the sequence of the capillary positions were listed as follows.

- For the initialization process, the capillary tip moved on to the three points A, B, and C, and then the 2-D homogeneous transformation matrix $\hat{H}_{PQ}$ was calculated using the Eq. 1.
- The capillary tip moved above the center point of the pillar. The capillary tip moved down vertically, contacted the pillar, and baselevel detection of the Z axis, z_0, was performed.
- The 3-D homogeneous transformation matrix $\hat{H}_{PM}$ was updated using the parameters of $\hat{H}_{PQ}$ and z_0 was performed.
- The capillary entered the oocyte at a direction of 45 degrees toward the center of the oocyte. The capillary trajectory was started from the starting point S, the point away from the oocyte at a distance l_1.
- The capillary was stopped at the moment transmembrane penetration was detected by the QCR force sensor. For the robustness, we set the maximum traveling range. The speed of the insertion was 100 μm/s
- For the oocyte detection and pillar detection in the image fame, we used Hough transformation to roughly obtain the position. The entire motion sequence was attached as a supplementary material.

Figure 10 shows a representative result of the capillary insertion. The oocyte was placed on the cantilever tip and two glass capillaries approached, contacted, and penetrated to the oocyte membrane one by one. We measured the position of the

glass capillary from the encoder, the image intensity of the ROI, and the signal of the QCR force sensor. The control frequency was 100 Hz. For this experiment, the electrophysiological results are not obtained, therefore, we used the oocytes in which the gene primer was not introduced. These oocytes are also measured as a reference of the backyard current of TEVC, essential process for the quantification. For the visibility, the capillary was colored dark by the metal deposition by the sputtering. The result clearly illustrated that when the contact of the glass capillary occurred to the oocyte membrane, the image intensity started with fluctuation of the output. The signal of the force was increased after that with some delay. Until the penetration occurred, the image signals were still fluctuating, whereas the force signal was corresponded to the penetration depth. After the repulsive force was suddenly drop-down, we stopped the stage of the capillary insertion, which resulted in the capillary insertion with a small amount of the indentation depth. For more quantitative insertion with less damaged insertion of the capillary will be considered as our future work.

IV. CONCLUSION

We developed the microscopic manipulation platform compatible to TEVC experiment. The remarkable progresses and the novelty were as follows;

- By using the sequential coordination calibration technique, three-dimensional manipulations of the single cell like a Xenopus oocyte with the robot manipulators was achieved under the stereomicroscopy whose focal depth were shallow.
- By using both the image analysis and the highly sensitive, rigid QCR force sensor, shallow capillary insertion to the oocyte membrane was achieved. The image analysis was utilized to distinguish the contact whereas the QCR force sensor was utilized to detect the penetration. Although the force interaction was on the order of 1 μN, our system successfully provided the force feedback for the motion control of the manipulator.

The methods and results will be further utilized for the general and versatile robot manipulations of biological samples.

REFERENCES

[1] Moustris, G.P., Hiridis, S.C., Deliparaschos, K.M. and Konstantinidis, K.M., "Evolution of autonomous and semi-autonomous robotic surgical systems: a review of the literature," *International Journal of Medical Robotics and Computer Assisted Surgery*, 7: 375-392, 2011.

[2] Dörr, M., Fibinger, M.P.C., Last, D., Schmidt, S., Santos-Aberturas, J., Böttcher, D., Hummel, A., Vickers, C., Voss, M. and Bornscheuer, U.T., "Fully automatized high-throughput enzyme library screening using a robotic platform," *Biotechnology and Bioengineering*, 113: 1421-1432, 2016.

[3] Scheel, Olaf and Himmel, Herbert and Rascher-Eggstein, Gesa and Knott, Thomas, "Introduction of a Modular Automated Voltage-Clamp Platform and Its Correlation with Manual Human Ether-à-go-go Related Gene Voltage-Clamp Data," *ASSAY and Drug Development Technologies*, 9, 6, 600-607, 2011.

[4] Trachsel, DS, Tejada, MA, Groesfjeld Christensen, V, et al. Effects of trimethoprim–sulfadiazine and detomidine on the function of equine Kv11.1 channels in a two-electrode voltage-clamp (TEVC) oocyte model. *J Pharmacol Therap*. ,41, 536–545, 2018.

[5] Zhao, Chunqing and Huang, Qiu-Tang and Jia, Zhongqiang and Wu, Shenggan and Liu, Feifan and Wang, Yingnan and Song, Genmiao and Chang, Xiaoli, "The Potential Toxicological Evaluation of Fluxametamide on Zebrafish," Danio Rerio, 18, 2022.

[6] Guan, B., Chen, X., Zhang, H., "Two-Electrode Voltage Clamp. In: Gamper, N. (eds) Ion Channels. Methods in Molecular Biology," 998. Humana Press, Totowa, NJ, 2013.

[7] Yasunobu Okada, "Patch-clamp Techniques, from beginning to advanced protocols," *Springer*, 2012.

[8] Katrin Schnizler, Mike Küster, Christoph Methfessel and Michael Fejtl, "The Roboocyte: Automated cDNA/mRNA Injection and Subsequent TEVC Recording on Xenopus Oocytes in 96-Well Microtiter Plates," *Receptors and Channels*, 9, 1, 41-48, 2003.

[9] S. Watanabe, H. Sugiura, and F. Arai, "Stiffness Measurement of Organoids Using a Wide-Range Force Sensor Probe Fabricated Using a Quartz Crystal Resonator," *IEEE Robotics and Automation Letters*, 7, 2, 2535-2540, 2022.

[10] Satoshi Amaya, Hirotaka Sugiura, Bilal Turan, Shingo Kaneko, and Fumihito Arai, "A PIPETTE TIP INTEGRATED WITH A CAPACITIVE MICROSENSOR FABRICATED BY COMBINED 3D PRINTING AND MEMS PROCESS FOR CELL DETECTION AND TRANSPORTATION," *Proc. IEEE Micro Electro Mechanical Systems (MEMS)*, SN,BioMEMS II. 2024.

[11] Jianbo Shi and Tomasi, "Good features to track," 1994 Proceedings of *IEEE Conference on Computer Vision and Pattern Recognition,* USA, 593-600, 1994.

[12] J. Illingworth, J. Kittler, "A survey of the hough transform," *Computer Vision, Graphics, and Image Processing*, 44, 1, 87-116, 1988.

[13] Y. Murozaki, S. Sakuma and F. Arai, "Detection of multi-biosignal using a quartz crystal resonator based wide range load sensor with compact frequency counter," Proc. *IEEE/RSJ International Conference on Intelligent Robots and Systems (IROS)*, Daejeon, Korea, 5585-5590, 2016.